J Mol Model (2003) 9:290–297
DOI 10.1007/s00894-003-0145-x

ORIGINAL PAPER

Ian R. Bates · George Harauz

Molecular dynamics exposes α-helices in myelin basic protein

Published online: 24 July 2003

Abstract Molecular dynamics simulations of models of unmodified and deiminated MBP (myelin basic protein) have been performed on solvated structures with added counterions, for 10 ns using AMBER (assisted model building with energy refinement). The protein structures became extended, and a considerable number of α-helical segments formed spontaneously. The degree of molecular extension was greater in the deiminated species, and the α-helices were more transient. These structural disruptions may be operative in vivo during multiple sclerosis.

Keywords Myelin basic protein (MBP) · Mutagenesis · Deimination · Citrulline · Molecular dynamics · Electrostatic potentials · Protein structure

Introduction

Myelin basic protein (MBP) is a major protein of the myelin sheath of the central nervous system, and is primarily responsible for maintaining the stability of the sheath by holding together the opposing cytoplasmic leaflets of the oligodendrocyte membrane. [1, 2] The MBP family comprises numerous developmentally regulated isoforms, of which the 18.5-kDa species is the most abundant in adult human and bovine myelin. This isoform undergoes numerous post-translational modifications, giving rise to charge isomers designated as components C1 to C8. [2, 3, 4] A post-translational modification of MBP that correlates with the severity of the disease multiple sclerosis is deimination, the enzymatic conversion of arginine to citrulline (Cit) by peptidylarginine deiminase (EC 3.5.3.15). [5, 6, 7, 8] Deimination reduces the net positive charge of the protein, yielding the C8 component, and limits its ability to maintain a compact myelin sheath by disrupting its interactions with lipids. [9, 10, 11, 12, 13, 14]

Deimination is an irreversible modification, and has been demonstrated to be an operative mechanism not only in the progression of multiple sclerosis, where MBP is modified, but also in other autoimmune disease states such as rheumatoid arthritis, where filaggrin is modified. [15, 16, 17, 18] Deimination has been shown by CD spectroscopy and other in vitro methods to disrupt the structure of MBP, [9, 11, 19, 20] and of other proteins such as trichohyalin. [21, 22] A three-dimensional model of human 18.5-kDa MBP (hMBP, human MBP) has been postulated, based on electron microscopic and other data, [23, 24] and is available as entry 1QCL in the Protein Data Bank. [25] Previously, we have performed molecular dynamics on this MBP model to assess the structural effects of deimination and methylation. [19, 20] Deimination, in particular, caused the protein structure to become less compact. However, for reasons of restricted computing resources at that time, these simulations were performed in vacuo only for a trajectory of 10 ps. In this paper, we report new molecular dynamics simulations for a 10-ns trajectory, using a more appropriate force-field, on a solvated protein model in the presence of counterions, in order to assess more rigorously the effects of deimination on MBP structure.

In the past few years, our laboratory has begun working with a recombinant form of murine 18.5-kDa MBP (rmMBP, recombinant murine MBP). [26] Since there is no known codon for Cit, we have used site-directed mutagenesis to convert selected arginyl/lysyl to glutaminyl residues. [27] The substituted amino acids corresponded to those six arginyl residues in the human protein that were most commonly deiminated in multiple sclerosis. The resulting recombinant protein was shown

I. R. Bates
Department of Molecular Biology and Genetics,
and Biophysics Interdepartmental Group,
University of Guelph, 50 Stone Road East, Guelph,
Ontario, N1G 2W1, Canada

G. Harauz (✉)
Department of Molecular Biology and Genetics,
University of Guelph, 50 Stone Road East, Guelph,
Ontario, N1G 2W1, Canada
e-mail: gharauz@uoguelph.ca
Tel.: +1 519-824-4120 x52535
Fax: +1 519-837-2075

by various biochemical and biophysical probes to mimic effectively the naturally deiminated protein. [27, 28] In the present work, we use molecular dynamics to address also the question of whether Arg/Lys→Gln substitution has the same apparent structural effects as Arg→Cit conversion.

Our nomenclature for these various protein species is as follows: C1 represents the 18.5-kDa isoform of murine MBP (mMBP) with no post-translational modifications; C8 represents C1 with six Arg/Lys→Cit conversions; qC8 represents C1 with six Arg/Lys→Gln substitutions to emulate deimination, i.e., quasi-C8. The net charges at neutral pH are +20, +14, and +14 for C1, C8, and qC8, respectively. The general name "mMBP" will be used to refer to C1, C8, or qC8 equivalently. The names hMBP and bovine MBP (bMBP) will be used to refer specifically to the human and bovine 18.5-kDa proteins, respectively. The human (170 residues), bovine (169 residues), and murine (168 residues) sequences of 18.5-kDa MBP are almost completely identical, with only a few gaps and conservative substitutions [viz., Fig. 1 in 27].

Materials and methods

Protein structures and software packages

The ab initio structure of the 18.5-kDa isoform of hMBP, entry 1QCL in the Protein Data Bank, [23, 24, 25] served as the reference to form a homology model of the 18.5-kDa isoform of mMBP, using the HOMOLOGY module of the INSIGHT2000 software package. [29] All subsequent minimization and dynamics steps were performed with the AMBER 6.0 program [30] using the all-atom force-field, also frequently referred to as AMBER. [31] The main modules from AMBER that were used were: SANDER (for energy minimization and molecular dynamics), XLEAP (graphical interface for building and linking molecules), and CARNAL (for analyzing structures and energies). [30]

The program CARNAL was used to calculate the root mean squared deviation (RMSD) of each simulated structure, from the initial configuration, over time. The radius of gyration of each simulated structure was also calculated over time using CARNAL. The potential energy, kinetic energy, and total energy over time were also extracted from the files of coordinates using CARNAL. The stereochemical anomalies remaining in the final structures of each simulation were evaluated using PROCHECK. [32] The electrostatic potentials of Arg, Gln, and Cit were visualized with the DELPHI module of INSIGHT2000 using the atomic partial charges (Fig. 1). [29] The images of the mMBP models were generated for presentation using DS ViewerPro 5.0. [29]

All AMBER simulations were run on two SGI ORIGIN 2000 servers (Silicon Graphics Inc., Mountainview, CA) with a total of four processors using the MPI implementation of SANDER. To verify the final structures, the simulations were replicated on servers with up to eight processors at the Ontario Center for Genomic Computing (Hospital for Sick Children, Toronto, ON, Canada). The total CPU time required for each simulation was about 8.5 days on the ORIGINS with four processors, and about 5 days on the servers with eight processors.

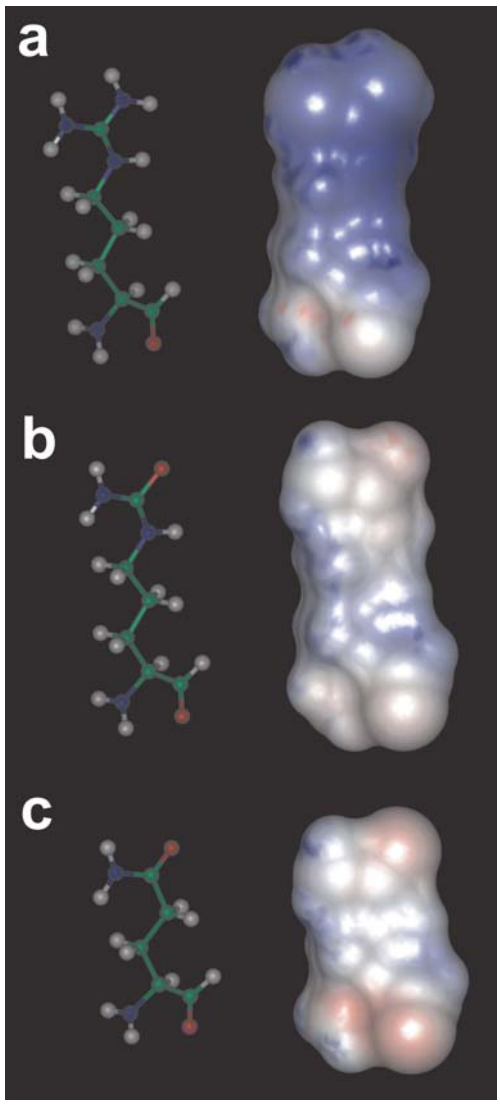

Fig. 1a–c Structures of **a** arginyl, **b** citrullinyl, and **c** glutaminyl residues, portrayed as ball and stick models (*left* panel) and as DELPHI-generated electrostatic distributions. A partial negative charge distribution is indicated in *red*, whereas a partial positive charge distribution is indicated in *blue*

Parameterization of citrulline

In order to simulate the structure of deiminated MBP, parameters for the non-standard citrullinyl residue needed to be developed. The amino acid Cit is quite similar to Arg, differing in the replacement of the amine group by an oxygen atom. (Essentially, Cit is a substituted urea.) This simple change, however, modifies the electrostatic potential of this residue (Fig. 1). Here, the structure of Cit

Table 1 Parameterization of citrulline in AMBER. Additional parameters are as follows: CA–O bond (K_r=570 kcal (mol Å^2)$^{-1}$, r_{eq}=1.229 Å), N2–CA–O angle (K_θ=80 kcal (mol radian^2)$^{-1}$, θ_{eq}=122.9°)

Atom name	Atom type	Bond length (Å)	Bond angle (°)	Torsion angle (°)	Partial atomic charge
N	N	1.335	116.6	180	–0.4157
H	H	1.01	119.8	0	0.2719
CA	CT	1.449	121.9	180	–0.0031
HA	H1	1.09	109.5	300	0.0850
CB	CT	1.525	111.1	60	–0.0036
HB2	HC	1.09	109.5	300	0.0171
HB3	HC	1.09	109.5	60	0.0171
CG	CT	1.525	109.47	180	–0.0645
HG2	HC	1.09	109.5	300	0.0352
HG3	HC	1.09	109.5	60	0.0352
CD	CT	1.525	109.47	180	0.0486
HD2	H1	1.09	109.5	300	0.0687
HD3	H1	1.09	109.5	60	0.0687
NE	N2	1.48	111.0	180	–0.5295
HE	H	1.01	118.5	0	0.3456
CZ	CA	1.33	123.0	180	0.6951
OH1	O	1.229	120.5	0	–0.6086
NH2	N	1.335	116.6	180	–0.9428
HE21	H	1.01	119.8	0	0.4251
HE22	H	1.01	119.8	180	0.4251
C	C	1.522	111.1	180	0.5973
O	O	1.229	120.5	0	–0.5679

was constructed within XLEAP by modifying an arginyl residue within the AMBER library. AMBER has a basis set of the bond, angle, and atomic charges for all standard amino acids. These data have been successfully employed in parameterizing other organic molecules, as well as modified amino acids. In this study, since Gln and Cit are both neutral in overall charge, the relevant partial charges of Gln were used to generate the electrostatic potential grid of Cit (Fig. 1, Table 1).

AMBER uses atom types to describe the hybridization of atoms as well as the details of the type of bonds and angles in which it is involved. The atom type that was chosen for the amino replacing oxygen was a carbonyl type with sp^2 hybridization (similar to that of Gln). This choice led to the problem of not having certain bond parameters, specifically the bond between an atom of type CA and an atom of type O. That particular configuration of Cit, where the zeta-carbon is bound to oxygen as well as a nitrogen atom of type N2, was not found in the AMBER parameter files. Thus, there was an unknown angle between atoms N2–CA–O. The parameters for C–O and N–C–O from AMBER's parm94.dat file were used to generate the appropriate bond and angle values for CA–O and N2–CA–O (Fig. 1, Table 1).

Energy minimization and molecular dynamics

An initial energy minimization of the mMBP model was performed to remove close van der Waals contacts. The modeling was performed in vacuo, with 200 steps of steepest descent followed by 500 steps of conjugate gradient. Initially, periodic boundary conditions were used to generate an 80 Å cube, with at least 8 Å separating the nearest protein residue from the edge of the box (Fig. 2). Approximately 12,500 water molecules were

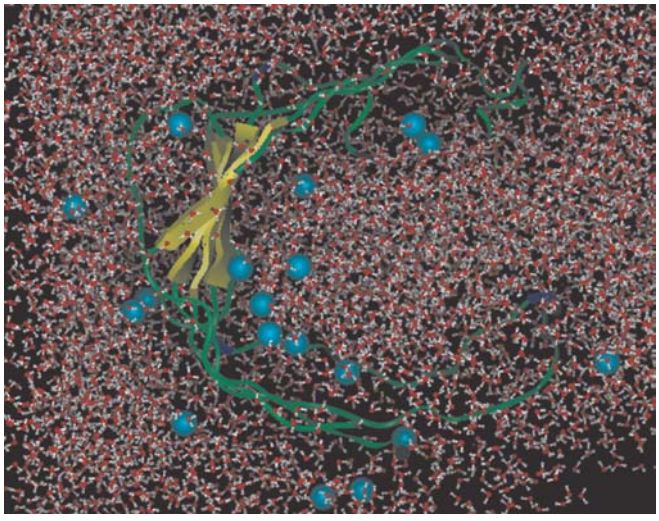

Fig. 2 Starting configuration of mMBP (homology-modeled from the 1QCL model of hMBP) within a cubic solvation box, and with added Cl^- counterions (*blue* spheres). The α-helices are colored *red*, the β-strands are colored *yellow*, the β-turns are colored *blue*, and random coils are colored *green*

then added to the system using the TIP3P water set, [33] which is employed by AMBER. This model is a pre-equilibrated set of water molecules with their own partial charges, permitting simulation of a biologically relevant interaction with the protein. To neutralize the high net positive charge of the C1 protein, 20 Cl^- ions were added to the system. (For C8 and qC8, 14 Cl^- ions were added.) Initial relaxation of the waters was done with 10 ps of minimization using a conjugate gradient approach, while keeping the protein structure fixed. This initial relaxation was then followed by 30 ps of minimization with protein and water molecules unrestricted.

For subsequent molecular dynamics simulations, the SHAKE option of SANDER was used to constrain the H–C, H–O, and H–N bonds (which have the highest frequency motions), allowing a time step of 2 fs. [34] The particle-mesh-Ewald (PME) method was used for the accurate determination of long-range electrostatic forces. [35, 36, 37, 38] For initial equilibration, constant pressure was used as well as a gradual warming protocol to raise the temperature slowly from 10 K to 300 K over 50 ps; the temperature was then held at 300 K for an additional 50 ps.

The subsequent simulations with mMBP were performed with constant volume and constant temperature up to 2 ns. At this point, the mMBP structure was found to be extending from the C-shape to a more flattened conformation, and the boundaries of the water cube were impeding further motion. The protein coordinates were then saved, and a new, longer water box was made and equilibrated. Another 8 ns of simulation were performed on this second system for a total trajectory of 10 ns.

Results

The most noticeable feature of all simulations, whose essential features were reproduced twice in independent molecular dynamics simulations, was the extensive structural deviation from the starting configurations (Fig. 3). Early in the simulation, the protein had visually become more extended than the original C-shape (compare Fig. 3 with Fig. 2). The RMSD increased sharply within the first 500 ps, fluctuated consistently for all forms of the protein up to about 8 ns, and appeared to be relatively stable for the last 2 ns (Fig. 4a). An additional parameter, the radius of gyration of each model, was also monitored. This value decreased suddenly at the start of the simulation (Fig. 4b), and fluctuated significantly until about 5 ns. From 5 to 10 ns, the radii of gyration of C8 and qC8 became comparable in magnitude (of the order of 20 Å) and greater than for C1 (of the order of 19 Å), indicating a greater degree of extension of the deiminated forms. The degree of fluctuation in this parameter is comparable to other results in the literature. [39, 40] By the end of the molecular dynamics runs, the numerous stereochemical anomalies present in the original structures, as ascertained by PROCHECK, had also been almost completely resolved (results not shown).

Since the original solvation cube size of 80 Å was impeding the continued extension of the protein, the MBP coordinate file at 2 ns was re-equilibrated within another water box with one side lengthened to accommodate the continued flattening of the molecule. The new system was run for another 8 ns after equilibration, and we consider structural equilibrium to have been reached.

Another interesting feature of this simulation was the *spontaneous* formation of small α-helices after the first 1 ns of simulation. Many of these α-helices were transient in nature, dissolving into random coil, and then reforming. The transitory nature of the α-helices explains, in part, the fluctuation of the radius of gyration (Fig. 4b). The most stable α-helices were considered to be the ones remaining in the final 1 ns of each simulation. In C1, there were numerous α-helical segments comprising residues mMBP(74–77), mMBP(118–122), mMBP(127–129), and mMBP(141–144). Of these structures, mMBP(118–122), mMBP(127–129), and mMBP(141–144) were amphipathic. The primary α-helical segments are shown in an enlarged representation of the final C1 model (Fig. 5).

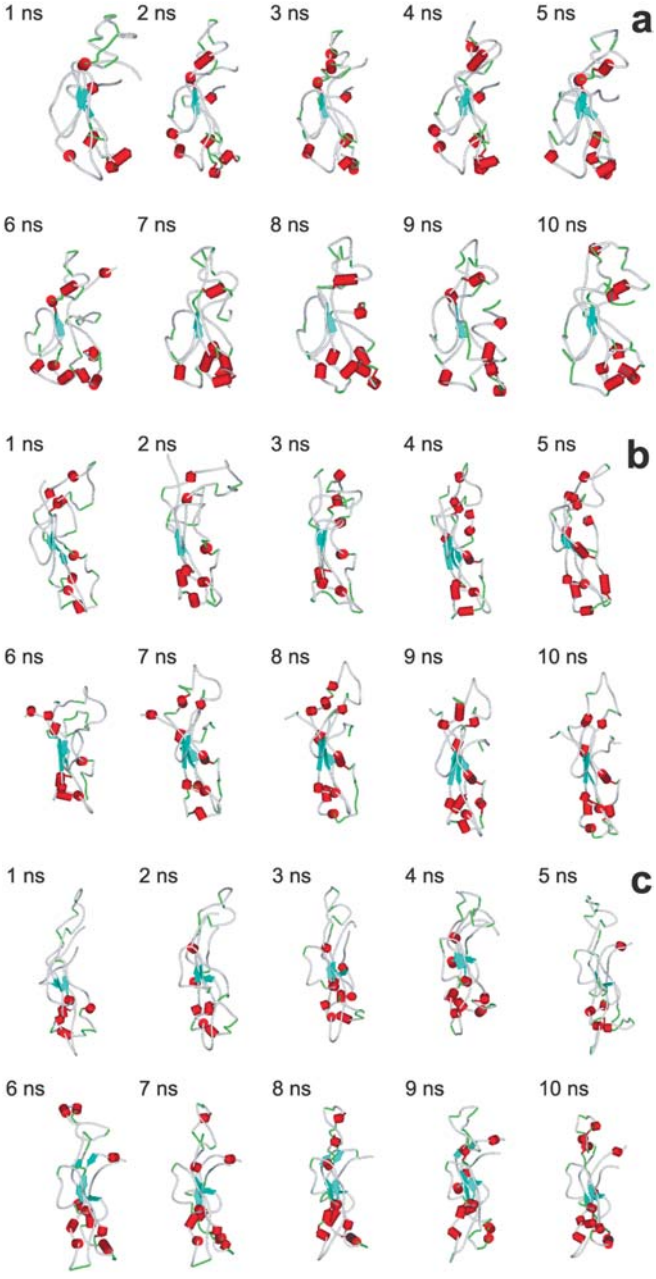

Fig. 3a–c Structural changes of mMBP species **a** C1, **b** C8, and **c** qC8 from starting configurations, as a function of time. The α-helices are colored *red*, the β-strands are colored *turquoise*, and the β-turns are colored *green*

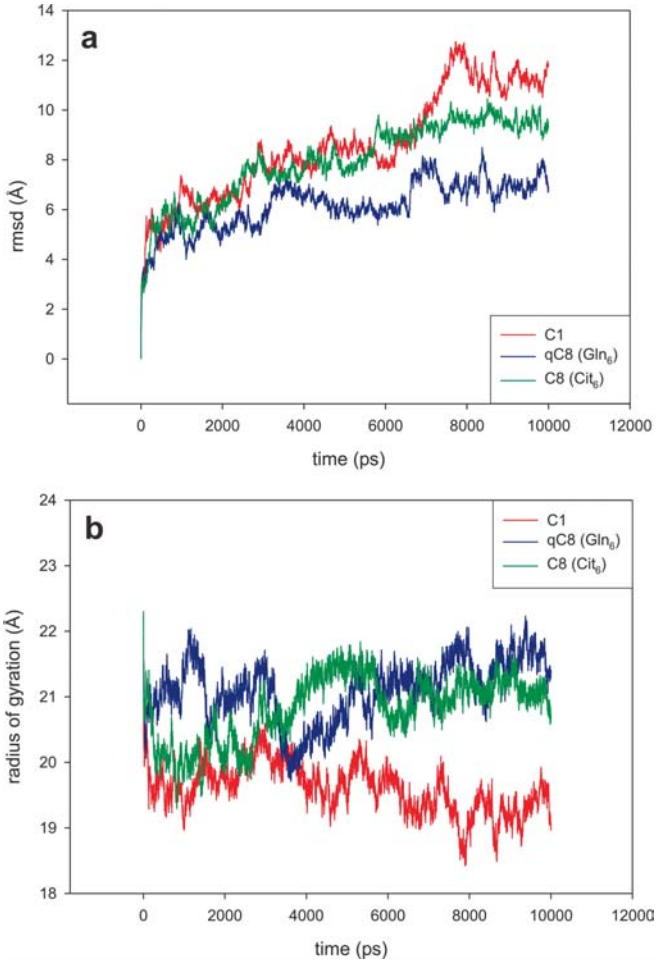

Fig. 4 **a** Root mean squared deviations, and **b** radii of gyration, of mMBP species C1, C8, and qC8 from starting configurations, as a function of time

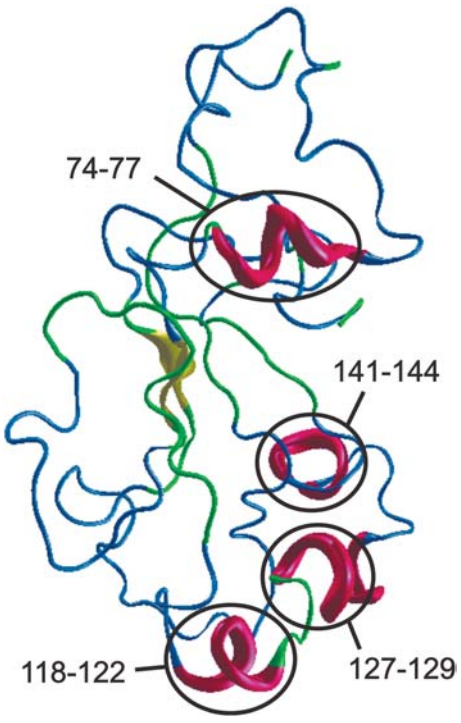

Fig. 5 Enlarged representation of the final C1 model, showing major α-helical segments that were stable over the last 1 ns of simulation. The α-helices are colored *red*, the β-strands are colored *yellow*, the β-turns are colored *blue*, and random coils are colored *green*

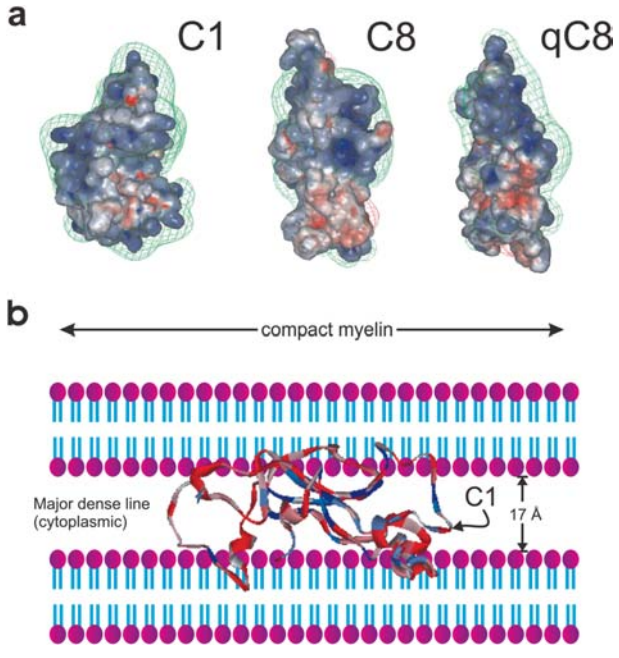

Fig. 6 **a** Models of mMBP species C1, C8, and qC8. Both charge distributions (from DELPHI) and Connolly surfaces (wire mesh) are shown. A partial negative charge distribution is indicated in *red*, whereas a partial positive charge distribution is indicated by *blue*. **b** Model for orientation of MBP within the major dense line of the myelin sheath

In C8 and qC8, the α-helices were generally more variable and ephemeral, with the most stable ones comprising residues mMBP(29–32) and mMBP(142–146) in C8, and residues mMBP(30–33) and mMBP(140–143) in qC8. The α-helices mMBP(142–146) in C8, and mMBP(140–143) in qC8, were amphipathic. Thus, the quasi-deiminated model behaved almost identically to the deiminated one. A further effect of deimination, both real and quasi, was that the global shapes of the proteins were different. In contrast to C1, both C8 and qC8 were almost completely extended into flattened rods (Fig. 6a).

Discussion

The 1QCL model of MBP

The atomic structure of MBP has not yet been determined by direct means such as X-ray crystallography or NMR, although a multidimensional NMR determination is presently under way. [41] The 1QCL model of hMBP

that we have created [23, 24] is based on numerous theoretical and experimental considerations. Phylogenetic sequence comparisons have indicated that there are conserved regions in MBP that are capable of forming an antiparallel β-sheet. [42, 43, 44, 45] Diverse experimental data over the decades [23, 46, 47, 48, 49, 50, 51, 52] indicate a thin, extended protein roughly 15 nm long. In electron micrographs of bovine and human MBP adsorbed to G_{M1}-containing lipid monolayers, the protein had a C-shape. [23] All of these considerations were incorporated into our construction of an atomic model of human MBP. [24] Since a C-shaped structure was a consequence of the experimental conditions and clearly cannot fit within the major dense line of the myelin sheath in vivo, [47, 53] we rationalize that this flexible protein must be extended to fit between the oligodendrocyte membrane leaflets. Although details of this MBP model will almost certainly change as high-resolution structural details become revealed, [41, 54] the model is correct in satisfying many aspects of MBP's known properties, including that of it being an "intrinsically unstructured" or "natively unfolded" protein. [55, 56] Thus, the 1QCL structure can be used to evaluate the potential effects of post-translational modifications, for example, and remains the only MBP model available for this purpose. [57]

Molecular dynamics simulations of protein models can provide insights to complement experimental data, [58] and denatured proteins have even been refolded into their native states *in silico*. [59, 60] The 1QCL model of hMBP has previously been used to evaluate the effects of deimination of arginyl residues, as well as mono- and symmetrical dimethylation of Arg107 on the structure. [19, 20] Two levels of deimination were evaluated: deimination of Arg25, Arg33, Arg122, Arg130, Arg159, and Arg170 (human sequence numbering) as found in the common, chronic form of multiple sclerosis, [3] and deimination of all 19 arginyl residues to emulate the form of hMBP found in the fulminating form of multiple sclerosis known as Marburg's syndrome. [6] Molecular dynamics were performed using INSIGHTII-97 molecular modeling software (Molecular Simulations, Inc., San Diego, Calif.) and the extensible and systematic force-field (ESFF). In particular, the deimination resulted in a relative increase in volume of the protein, and greater exposure of cathepsin D binding sites, as seen biochemically. [19] In myelin in vivo, the protein would thus be more exposed and more susceptible to autoimmune or proteolytic attack. Similarly, computational methylation of Arg107 resulted in sequestration of this residue into the backbone β-sheet and a perturbation of overall protein structure. [20] Unfortunately, the restricted computing power available to us at that time precluded simulations longer than a 10-ps trajectory, and only the unhydrated protein could be modeled in vacuo.

Molecular dynamics simulations of short duration do not, in general, become fully equilibrated. [61] It is now standard for simulations to extend for trajectories of nanoseconds. [62] Moreover, it is essential to include other physiologically relevant biological molecules (waters, ions) in the system as possible. [40, 63, 64, 65, 66] With these considerations in mind, the simulations presented here have been extended for a trajectory several magnitudes longer: 10 ns compared to 10 ps. We have included 12,500 explicit water molecules, which not only interact with the protein via polar contacts and non-polar repulsion, but also have a charge shielding effect due to the dielectric properties of bulk water. The result is a more realistic dynamic simulation than simply assigning a dielectric screening term. [63] Further charge shielding was achieved by the presence of Cl^- ions, as would be found in the natural milieu. In addition, the AMBER force-field is superior for highly charged proteins; it uses quantum mechanical methods to derive the electrostatic potential of the protein, and a modified point charge fitting method called "restrained electrostatic potential". [30, 31] Moreover, AMBER enables better handling of long-range electrostatic effects using the PME technique. [35, 36, 37, 38]

Structural changes and α-helix formation over time

The most noticeable feature of all simulations was that each protein species became more extended from its original C-shape (Figs. 2 and 3), which makes sense from a biological perspective. The flattened protein would fit easily within the narrow confines of the major dense line (Fig. 6b). There was a greater degree of extension of the deiminated forms of the protein, which may shed some light on its altered interactions with lipids, and with ligands such as calmodulin. Firstly, the more compact shape of C1 might serve to concentrate charge over a smaller area, in contrast to C8 and qC8, where the reduced charge would be distributed over a larger region. Secondly, we have shown in our laboratory that deiminated MBP interacts differently with calmodulin than the unmodified protein. [29] The latter has a primary calmodulin target at its carboxy terminus, and the binding stoichiometry is 1:1. The deiminated proteins (both real and quasi) appear to have additional, weaker calmodulin-binding sites, which we have postulated could be exposed by structural perturbations caused by this modification. The results obtained here with molecular dynamics simulations support this conjecture, since these sites could be one of the amphipathic α-helices that formed spontaneously during molecular dynamics simulations.

The original 1QCL model was minimalist in that it comprised only a β-sheet backbone, with the rest being modeled as loops. This backbone remained essentially intact in all simulations, demonstrating its overall stability. Here, we were intrigued to observe also the *spontaneous* formation of small α-helices after the first 1 ns of simulation. It is accepted that there are α-helical segments in MBP, especially after it interacts with detergents and lipids. [reviewed in 67] Stoner [43] proposed an MBP model with two α-helices, in order to permit the shielding of hydrophobic residues. One of these was segment

mMBP(133–144), which corresponds here to the preliminary formation of an α-helix comprising mMBP(138–144)=FLGATNA. However, this helix is not completely formed in the molecular model, and it appears to have a bend at the glycyl residue (which is to be expected from physicochemical considerations). Here, the fleeting nature of many of the α-helices may also only occur in aqueous solution; in vivo, they could be stabilized by their interactions with lipids, [67] or by post-translational modifications. [68] Future molecular dynamics simulations in mixed 2,2,2-trifluoroethanol–water mixtures [69] for even longer trajectories [39, 70] would stabilize these structures *in silico* as well.

Many proteins use amphipathic α-helices to stabilize their interactions with membranes, and several segments of MBP with the potential to form amphipathic or other α-helices have previously been identified. [67, 71, 72, 73] There is a very good correspondence between our results and those of Mendz et al. [71], who demonstrated experimentally the formation of α-helices in short peptide fragments of MBP in the presence of lipids. The work of Polverini et al. [67] is noteworthy in that it utilized ten of the most common secondary structure prediction tools then available. They predicted seven stable segments of bMBP: I (9–24, β or α), II (35–43, β), III (61–67, α), IV (85–93, β), V (107–115, β), VI (131–139, α), and VII (146–155, β), with segments IV and V being the most consistently predicted, and, therefore, thought to be the most stable. Given the uncertainties inherent in any structure prediction method, [74] there is a reasonable correspondence with the predictions of Polverini et al. [67] and the spontaneous formation of α-helices observed here after molecular dynamics. The stable (in C1) α-helical segment comprising residues mMBP(74–77) matches their predictions of helical propensity around residue 74, and is quite close to their segment III. In addition, the stable and amphipathic α-helical segment comprising residues mMBP(141–144) appeared after 1 ns and remained intact until 10 ns, and is physically close to their segment VI. These results collectively suggest that the formation of α-helices in MBP is necessary to alleviate hydrophobic forces and stabilize the tertiary structure.

Deimination serves to disfavor formation of these otherwise stable α-helices, in agreement with CD data that show that less ordered secondary structure is induced by lipids in modified than in unmodified MBP. [27, 28] There was no consistent correlation between deimination sites and "lost" α-helices, so the effect of this post-translational modification appears to be collective. Here, Arg/Lys→Gln substitutions appeared to have the same effect as Arg/Lys→Cit conversions, despite the smaller physical size of the Gln. [cf., 75]

Finally, it should be pointed out that the α-helices that formed here spontaneously arose only in regions that were originally random coil. The β-sheets appeared here to be quite stable. However, an electron paramagnetic resonance study in our laboratory indicates that segment mMBP(83–92) is probably an amphipathic α-helix that lies on the surface of the lipid bilayer. [54] This segment overlaps a β-strand in the 1QCL model, and the non-covalent interactions prevented its appearance as an α-helix in the present molecular dynamics simulations. The discrepancy can be resolved by positing a $\beta\alpha\beta$ motif, [76] although a definitive resolution must await completion of an NMR structural determination that is presently in progress. [41]

Concluding remarks

Molecular dynamics simulations of models of several forms of mMBP, with added water molecules and counterions, have been performed using AMBER until equilibrium was reached. The protein structure became extended, and could readily fit into the major dense line of the myelin sheath. There was considerable formation of short α-helices, which would be stabilized in the presence of lipids and which could serve to anchor the protein to the myelin membrane. Deimination disfavored formation of these α-helical structures, and also caused the protein to become even less compact, consistent with experimental data and with our previous simulations. These results are the first demonstration, at the atomic level, of the effects of deimination on a protein. The net charge of the protein clearly has an effect on its tertiary structure, and the highly basic C1 form could be maintained in a more rigid conformation in vivo by long-range electrostatic interactions. The protein model comprising Arg/Lys→Gln substitutions appeared also to mimic the model with Arg/Lys→Cit conversions, supporting use of the former recombinant protein instead of the latter natural protein in some experiments. Future molecular dynamics simulations of the C1 species of MBP placed between two lipid bilayers will provide further insights into how this protein maintains and stabilizes the structure of the myelin sheath.

Acknowledgements This work was supported by grants from the Natural Sciences and Engineering Research Council of Canada, the Multiple Sclerosis Society of Canada, and the Canadian Institutes for Health Research. IRB was the recipient of a Multiple Sclerosis Society of Canada Studentship. The SGI servers and INSIGHT2000 software were purchased with the assistance of the Canada Foundation for Innovation. The authors are grateful to Mr. Len Zaifman of the Ontario Center for Genomic Computing for assistance with obtaining computer time and resources.

References

1. Smith R (1992) J Neurochem 59:1589–1608
2. Moscarello MA (1997) Myelin basic protein, the "executive" molecule of the myelin membrane. In: Juurlink BHJ, Devon RM, Doucette JR, Nazarali AJ, Schreyer DJ, Verge VMK (eds) Cell biology and pathology of myelin: evolving biological concepts and therapeutic approaches. Plenum, New York, pp 13–25
3. Wood DD, Moscarello MA (1997) Myelin basic protein—the implication of post-translational changes for demyelinating disease. In: Russell W (ed) The molecular biology of multiple sclerosis. Wiley, New York, pp 37–54

4. Zand R, Li MX, Jin X, Lubman D (1998) Biochemistry 37:2441–2449
5. Moscarello MA, Wood DD, Ackerley C, Boulias C (1994) J Clin Invest 94:146–154
6. Wood DD, Bilbao JM, O'Connors P, Moscarello MA (1996) Ann Neurol 40:18–24
7. Tranquill LR, Cao L, Ling NC, Kalbacher H, Martin RM, Whitaker JN (2000) Mult Scler 6:220–225
8. Moscarello MA, Pritzker L, Mastronardi FG, Wood DD (2002) J Neurochem 81:335–343
9. Lamensa JW, Moscarello MA (1993) J Neurochem 61:987–996
10. Boggs JM, Rangaraj G, Koshy KM, Ackerley C, Wood DD, Moscarello MA (1999) J Neurosci Res 57:529–535
11. Cao L, Goodin R, Wood D, Moscarello MA, Whitaker JN (1999) Biochemistry 38:6157–6163
12. Beniac DR, Wood DD, Palaniyar N, Ottensmeyer FP, Moscarello MA, Harauz G (2000) J Struct Biol 129:80–95
13. Ishiyama N, Bates IR, Hill CM, Wood DD, Matharu P, Viner NJ, Moscarello MA, Harauz G (2001) J Struct Biol 136:30–45
14. Ishiyama N, Hill CM, Bates IR, Harauz G (2002) Chem Phys Lipids 114:103–111
15. Schellekens GA, de Jong BA, van den Hoogen FH, van de Putte LB, van Venrooij WJ (1998) J Clin Invest 101:273–281
16. Girbal-Neuhauser E, Durieux JJ, Arnaud M, Dalbon P, Sebbag M, Vincent C, Simon M, Senshu T, Masson-Bessière C, Jolivet-Reynaud C, Jolivet M, Serre G (1999) J Immunol 162:585–594
17. van Venrooij WJ, Pruijn GJ (2000) Arthritis Res 2:249–251
18. Reparon-Schuijt CC, van Esch WJ, van Kooten C, Schellekens GA, de Jong BA, van Venrooij WJ, Breedveld FC, Verweij CL (2001) Arthritis Rheum 44:41–47
19. Pritzker LB, Joshi S, Gowan JJ, Harauz G, Moscarello MA (2000) Biochemistry 39:5374–5381
20. Pritzker LB, Joshi S, Harauz G, Moscarello MA (2000) Biochemistry 39:5382–5388
21. Tarcsa E, Marekov LN, Mei G, Melino G, Lee SC, Steinert PM (1996) J Biol Chem 271:30709–30716
22. Tarcsa E, Marekov LN, Andreoli J, Idler WW, Candi E, Chung SI, Steinert PM (1997) J Biol Chem 272:27893–27901
23. Beniac DR, Luckevich MD, Czarnota GJ, Tompkins TA, Ridsdale RA, Ottensmeyer FP, Moscarello MA, Harauz G (1997) J Biol Chem 272:4261–4268
24. Ridsdale RA, Beniac DR, Tompkins TA, Moscarello MA, Harauz G (1997) J Biol Chem 272:4269–4275
25. Berman HM, Battistuz T, Bhat TN, Bluhm WF, Bourne PE, Burkhardt K, Feng Z, Gilliland GL, Iype L, Jain S, Fagan P, Marvin J, Padilla D, Ravichandran V, Schneider B, Thanki N, Weissig H, Westbrook JD, Zardecki C (2002) Acta Crystallogr, Sect D 58:899–907;http://www.rcsb.org/pdb
26. Bates IR, Matharu P, Ishiyama N, Rochon D, Wood DD, Polverini E, Moscarello MA, Viner NJ, Harauz G (2000) Protein Expr Purif 20:285–299
27. Bates IR, Libich DS, Wood DD, Moscarello MA, Harauz G (2002) Protein Expr Purif 25:330–341
28. Libich DS, Hill CMD, Bates IR, Hallett FR, Armstrong S, Siemiarczuk A, Harauz G (2003) Prot Sci 12:1507–1521
29. INSIGHT2000 / DS ViewerPro 5.0 (2000) Accelrys Inc, San Diego, CA, USA;http://www.accelrys.com
30. Pearlman DA, Case DA, Caldwell JW, Ross WS, Cheatham TE, Debolt S, Ferguson D, Seibel G, Kollman P (1995) Comput Phys Commun 91:1–41
31. Cornell WD, Cieplak P, Bayly CI, Gould IR, Merz KM, Ferguson DM, Spellmeyer DC, Fox T, Caldwell JW, Kollman PA (1995) J Am Chem Soc 117:5179–5197
32. Laskowski RA, MacArthur MW, Moss DS, Thornton JM (1993) J Appl Crystallogr 26:283–291
33. Jorgensen WL, Chandrasekhar J, Madura JD, Imprey RW, Klein ML (1983) J Chem Phys 79:926–935
34. Ryckaert JP, Ciccotti G, Berendsen HJC (1977) J Comput Phys 23:327–341
35. Darden T, York D, Pedersen L (1993) J Chem Phys 98:10089–10092
36. Essmann U, Perera L, Berkowitz ML, Darden T, Lee H, Pedersen LG (1995) J Chem Phys 103:8577–8593
37. Fox T, Kollman PA (1996) Proteins 25:315–334
38. Sagui C, Darden TA (1999) Annu Rev Biophys Biomol Struct 28:155–179
39. Duan Y, Kollman PA (1998) Science 282:740–744
40. Gerini MF, Roccatano D, Baciocchi E, Di Nola A (2003) Biophys J 84:3883–3893
41. Libich DS, Robertson VJ, Monette MM, Harauz G (2003) NMR investigations of the structure of myelin basic protein. In: Proceedings of the XIX International Congress of Biochemistry and Molecular Biology. Montreal, Canada, 8–11 October
42. Martenson RE (1981) J Neurochem 36:1543–1560
43. Stoner GL (1984) J Neurochem 43:433–447
44. Martenson RE (1986) J Neurochem 46:1612–1622
45. Stoner GL (1990) J Neurochem 55:1404–1411
46. Epand RM, Moscarello MA, Zierenberg B, Vail WJ (1974) Biochemistry 13:1264–1267
47. Sedzik J, Blaurock AE, Höchli M (1984) J Mol Biol 174:385–409
48. MacNaughtan W, Snook KA, Caspi E, Franks NP (1985) Biochim Biophys Acta 818:132–148
49. Afshar-Rad T, Bailey AI, Luckham PF, MacNaughtan W, Chapman D (1987) Biochim Biophys Acta 915:101–111
50. Haas H, Torrielli M, Steitz R, Cavatorta P, Sorbi R, Fasano A, Riccio P, Gliozzi A (1998) Thin Solid Films 329:627–631
51. Haas H, Torrielli M, Steitz R, Cavatorta P, Sorbi R, Fasano A, Zito F, Riccio PA, Gliozzi A (1999) Ital J Biochem 48:193-194
52. Mueller H, Butt HJ, Bamberg E (1999) Biophys J 76:1072–1079
53. Riccio P, Fasano A, Borenshtein N, Bleve-Zacheo T, Kirschner DA (2000) J Neurosci Res 59:513–521
54. Bates IR, Boggs JM, Feix JB, Harauz G (2003) J Biol Chem 278:29041–29047
55. Hill CMD, Bates IR, White GF, Hallett FR, Harauz G (2002) J Struct Biol 139:13–26
56. Hill CMD, Haines JD, Antler CE, Bates IR, Libich DS, Harauz G (2003) Micron 34:25–37
57. Kursula P (2001) Int J Mol Med 8:475–479
58. Karplus M, Petsko GA (1990) Nature 347:631–639
59. Lee MR, Tsai J, Baker D, Kollman PA (2001) J Mol Biol 313:417–430
60. Lee MR, Duan Y, Kollman PA (2001) J Mol Graph Model 19:146–149
61. Daggett V (2000) Curr Opin Struct Biol 10:160–164
62. Hansson T, Oostenbrink C, van Gunsteren W (2002) Curr Opin Struct Biol 12:190–196
63. Levitt M, Sharon R (1988) Proc Natl Acad Sci USA 85:7557–7561
64. Ibragimova GT, Wade RC (1998) Biophys J 74:2906–2911
65. Ibragimova GT, Wade RC (1999) Biophys J 77:2191–2198
66. Pfeiffer S, Fushman D, Cowburn D (1999) Proteins 35:206–217
67. Polverini E, Fasano A, Zito F, Riccio P, Cavatorta P (1999) Eur Biophys J 28:351–355
68. Andrew CD, Warwicker J, Jones GR, Doig AJ (2002) Biochemistry 41:1897–1905
69. Roccatano D, Colombo G, Fioroni M, Mark AE (2002) Proc Natl Acad Sci USA 99:12179–12184
70. Gnanakaran S, Nymeyer H, Portman J, Sanbonmatsu KY, Garcia AE (2003) Curr Opin Struct Biol 13:168–174
71. Mendz GL, Moore WJ, Brown LR, Martenson RE (1984) Biochemistry 23:6041–6046
72. Mendz GL, Brown LR, Martenson RE (1990) Biochemistry 29:2304–2311
73. Mendz GL, Miller DJ, Ralston GB (1995) Eur Biophys J 24:39–53
74. Rost B (2001) J Struct Biol 134:204–218
75. Jantz D, Berg JM (2003) J Am Chem Soc 125:4960–4961
76. Warren KG, Catz I, Steinman L (1995) Proc Natl Acad Sci USA 92:11061–11065